

Electron-nucleus spin correlation conservation of the spin dependent recombination in Ga^{2+} centers.

J. C. Sandoval-Santana,¹ V. G. Ibarra-Sierra,² H. Carrère,³ L.A. Bakaleinikov,⁴ V. K. Kalevich,⁴ E. L. Ivchenko,⁴ X. Marie,³ T. Amand,³ A. Balocchi,³ and A. Kunold⁵

¹*Instituto de Física, Universidad Nacional Autónoma de México, Apartado Postal 20-364 01000, Ciudad de México, México*

²*Departamento de Sistemas Complejos, Instituto de Física, Universidad Nacional Autónoma de México, Apartado Postal 20-364, 01000, Ciudad de México, México.*

³*Université de Toulouse, INSA-CNRS-UPS, LPCNO, 135 avenue de Rangueil, 31077 Toulouse, France*

⁴*Ioffe Physical-Technical Institute, 194021 St. Petersburg, Russia*

⁵*Área de Física Teórica y Materia Condensada, Universidad Autónoma Metropolitana Azcapotzalco, Av. San Pablo 180, Col. Reynosa-Tamaulipas, 02200 Ciudad de México, México*

Spin dependent recombination in GaAsN offers many interesting possibilities in the design of spintronic devices mostly due to its astounding capability to reach conduction band electron spin polarizations close to 100% at room temperature. The mechanism behind the spin selective capture of electrons in Ga^{2+} paramagnetic centers is revisited in this paper to address inconsistencies common to most previously presented models. Primarily, these errors manifest themselves as major disagreements with the experimental observations of two key characteristics of this phenomenon: the effective Overhauser-like magnetic field and the width of the photoluminescence Lorentzian-like curves as a function of the illumination power. These features are not only essential to understand the spin dependent recombination in GaAsN, but are also key to the design of novel spintronic devices. Here we demonstrate that the particular structure of the electron capture expressions introduces spurious electron-nucleus correlations that artificially alter the balance between the hyperfine and the Zeeman contributions. This imbalance strongly distorts the effective magnetic field and width characteristics. In this work we propose an alternative recombination mechanism that preserves the electron-nucleus correlations and, at the same time, keeps the essential properties of the spin selective capture of electrons. This mechanism yields a significant improvement to the agreement between experimental and theoretical results. In particular, our model gives results in very good accord with the experimental effective Overhauser-like magnetic field and width data, and with the degree of circular polarization under oblique magnetic fields.

I. INTRODUCTION

Spin dependent recombination (SDR) has been studied extensively, both experimentally and theoretically because of the many possibilities it offers to the design of spintronic devices¹⁻²⁹. SDR was first observed in silicon¹⁻³ and later in GaAsN alloys with a small content of nitrogen^{4,6}. It relies on the Pauli principle that states that two electrons cannot occupy simultaneously a quantum level with the same spin orientation. Hence, the capture rate in a paramagnetic center is strongly influenced by the relative spin orientation of the conduction band (CB) electrons and the centers outer shell electrons. More specifically, the recombination when both electrons have opposite spin orientations will have significantly faster capture rates than those with parallel orientation⁴⁻⁶. This difference gives rise to a spin filtering process where photogenerated electrons are either fastly recombined, if they have opposite spin orientation to the centers, or remain for very long times in the CB if they have opposing spin orientations^{8,9,15}. The spin filtering effect along with the particular selection rules of GaAs enable to control the degree of CB electron spin polarizations through optically oriented pumping over a wide energy excitation range³⁰. The most staggering outcome of this dynamical process is the large CB electron spin polarization of almost 100%²³ that can be attained

at room temperature. Moreover, the presence of large CB electron populations, sustained by the spin filtering effect, considerably increase the photoconductivity under the incidence of circularly polarized light. This allows for the detection of the CB electrons degree of spin polarization^{12,16}.

It is widely accepted that in GaAsN dilute semiconductors, it is primarily Ga^{2+} interstitial centers that play the role of paramagnetic traps and spin filtering defects^{9,13,18,28}. Experimental findings on GaAsN showed an improvement of the spin filtering effect, as an increase the photoluminescence (PL) intensity or the the degree of circular polarization (DCP) of the emitted light under a moderate (100mT) Faraday configuration magnetic field^{17,19-21}. Specifically, the PL intensity $J(B_z)$ or the DCP $P_e(B_z)$ of the emitted light as a function of the longitudinal magnetic field B_z take the shape of an inverted Lorentzian functions as can be seen in Fig. 1 (a). The primary cause of this phenomenon was identified as the hyperfine interaction (HFI) between the bounded electrons and the corresponding nuclei in Ga^{2+} centers^{20-23,25}. The shape of $J(B_z)$ and $P_e(B_z)$ emerges from the competition between the hyperfine and the Zeeman interactions. In the low magnetic field regime the HFI is dominant, but as the magnetic field increases and the Zeemna interaction becomes stronger, bound electrons and nuclei decouple. At this stage the angular mo-

momentum transfer and mixing between electrons and nuclei induced by the HFI is interrupted and the spin filtering effect becomes more efficient^{22,25}. This alone can not fully explain the amplification of the spin filtering effect. The nuclear spin relaxation, dominated by the dipolar interaction between neighbouring nuclei²⁵, also contributes to the amplification of the spin filtering effect. In fact, in its absence, the increase in the DCP of the PL would not be observable²⁵. The interplay between the HFI and the spin relaxation produces an effective Overhauser-like magnetic field that manifests as a shift of a few tens of mT of the minimum of $J(B_z)$ and $P_e(B_z)$ with respect to $B_z = 0$ mT¹⁹ as can be seen in Fig. 1 (a). This shift is a distinctive property of centers with nuclear spin $I > 1/2$ as it is the case for Ga^{2+} ($I^{Ga} = 3/2$)^{3,23,24}. Furthermore, the effective magnetic field is sensitive to the orientation of the circularly polarized light: the incidence of left circularly polarized light displaces the curves to the positive \rightarrow negative magnetic field region and right circularly polarized light to the positive region.

To fully exploit this properties in spintronic devices, it is of great importance to completely comprehend the mechanisms behind the complex behaviour of Ga^{2+} centers. Hitherto, experimental results on PL and DCP under circularly polarized light in different magnetic field configurations have been correctly reproduced by four theoretical models^{20,22,24,25} (a brief summary of them together with the sample characteristics and experimental conditions can be found in Ref. [25]). However, not even the most general of these models²⁵ is able to capture two important features: the effective magnetic field and the width of the $J(B_z)$ and $P_e(B_z)$ curves as a function of the power of the incident light. Whereas, experimental results yield a monotonically increasing effective magnetic field B_e as a function of the illumination power until it saturates at approximately 25mT¹⁹, the theoretical results give a vanishing effective magnetic field in the high power regime²⁵. In Fig. 1 (b) we have superimposed the experimental (solid circles) and theoretical (solid line) behaviours of the effective magnetic field B_e as functions of the illumination power. Likewise, the width $B_{1/2}$ of the $J(B_z)$ and $P_e(B_z)$ experimental curves consist of monotonically decreasing functions of power that saturate at approximately 100mT. The theoretical model gives instead a monotonically increasing function of power that never saturates. This can be observed in Fig. 1 (c), where we have plotted the experimental (solid circles) and theoretical (solid line) curves of $B_{1/2}$ vs. power intensity. Since the two features, the width and the shift (the effective magnetic field), parametrize the DCP of the emitted light and its orientation, understanding their origin is a crucial step towards the design of GaAsN spintronic devices.

In this work we develop a model for the SDR in Ga^{2+} centers that correctly accounts for the experimental behaviour of the width and the shift of the $J(B_z)$ and $P_e(B_z)$ curves. It is shown that the recombination processes considered in previous models^{20,24,25} is incor-

rect because it artificially introduces correlations between bound electrons and nuclei in G^{2+} centers. The proposed new SDR mechanism correctly describes other experiments that are very sensitive to width and the shift, as the DCP of the photoluminescence in GaAsN samples subject to tilted magnetic fields.

The paper is organized as follows. Section II is divided in several subsections where the master equation and its multiple elements are introduced. First we briefly review the master equation approach adopted to model the spin dynamics of GaAsN bulk alloy in section II A. Section II B deals with the Lie algebraic method used to build the dissipators corresponding to the VB hole and CB electron recombination processes. These are calculated in sections II C and II D. In section II D we address the SDR process. We show that previous versions of the SDR dissipator has problems that introduce artificially electron-nucleus spin correlations. In this section we propose a new SDR dissipator that solves this inconsistency. The comparison of the results produced by the new dissipator and experimental data is presented section III.

II. MODEL

A. The master equation for GaAsN

For the sake of completeness, as a starting point we briefly present the main elements of the master equation approach used in our previous works. The master equation is given by

$$\frac{d\rho}{dt} = \frac{i}{\hbar} [\rho, H] + \mathcal{D}(\rho), \quad (1)$$

where ρ is the density matrix, H is the Hamiltonian and \mathcal{D} is the dissipator. We consider the system as being formed of four subspaces: VB holes, CB electrons, singly occupied traps and doubly occupied traps. VB holes are considered to be unpolarized due to their fast spin relaxation time and CB electrons have the to possible spin projections of the spin. Singly occupied traps are Ga^{2+} centers whose 4s shell only has one electron with any of the two possible projections of spin. Doubly occupied traps, instead, are Ga^{2+} centers whose 4s shell if full and therefore cannot capture any additional electrons due to the Pauli principle. Provided that the coherences between the subspaces vanish, the density matrix can thus be expressed as the direct sum

$$\rho = \rho_v \oplus \rho_c \oplus \rho_1 \oplus \rho_2, \quad (2)$$

where ρ_v and ρ_c are valence and conduction band density matrices. The subspaces of singly and doubly occupied Ga^{2+} centers are described by the ρ_1 and ρ_2 density matrices. The Hamiltonian for the Zeeman and hyperfine couplings is given by

$$H = \hbar\omega \cdot \mathbf{S} + \mathbf{\Omega} \cdot \mathbf{S} + A\mathbf{I}_1 \cdot \mathbf{S}_c, \quad (3)$$

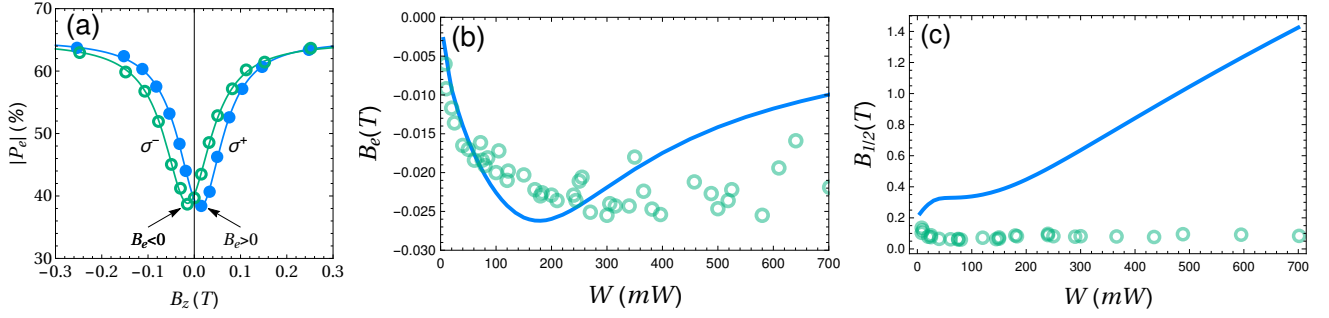


Figure 1. (a) Experimental behaviour of the degree of circular polarization P_e as a function of the longitudinal magnetic field B_z under right (σ^+) and left (σ^-) circularly polarized light. (b) Effective magnetic field B_e as a function of the illumination power. (c) Mean width $B_{1/2}$ as a function of the illumination power. The purple solid circles correspond to the experimental results and the solid blue line are the theoretical calculations.

where A is the hyperfine parameter of Ga^{2+} centers, $\omega = g\mu_B\mathbf{B}/\hbar$, $\Omega = g_c\mu_B\mathbf{B}/\hbar$, μ_B is the Bohr magneton, \mathbf{B} is the external magnetic field, g is the gyromagnetic factor for CB electrons and g_c is the gyromagnetic factor for bound electrons in Ga^{2+} centers. \mathbf{S} and \mathbf{S}_c are the CB electrons and bound electrons spin operators. \mathbf{I}_1 and \mathbf{I}_2 are the nuclear spin operators of singly and doubly occupied Ga^{2+} centers. The dissipator is given by the sum of the following contributions

$$\mathcal{D}(\rho) = \mathcal{G} + \mathcal{D}_S + \mathcal{D}_{SC} + \mathcal{D}_1 + \mathcal{D}_2 + \mathcal{D}_P + \mathcal{D}_{SDR}. \quad (4)$$

The photogeneration of electron-hole pairs is described by the first term

$$\mathcal{G} = (G_+ + G_-)(p + n) + 2(G_+ - G_-)\mathbf{e} \cdot \mathbf{S}, \quad (5)$$

where $n = 2S_0$ is the number operator for CB electrons and \mathbf{e} is a unitary vector parallel to excitation direction. Spin-up and spin-down CB electron generation rates are given by the smooth step function

$$G_{\pm}(t) = \frac{G_0 W}{2} \frac{1 \pm P}{2} \left[1 + \tanh\left(\frac{t - t_0}{s_t}\right) \right], \quad (6)$$

where G_0 is the power generation factor, W is the excitation power $s_t = 10$ ps is the width of the step function and P is the spin polarization degree ($0 < P \leq 1$ generates mostly spin-up electrons and $-1 \leq P < 0$ spin-down electrons). The CB and bound electron spin relaxation are given by

$$\mathcal{D}_S = -\frac{1}{2\tau_s} \sum_{k=1}^3 [S_k, [S_k, \rho]], \quad (7)$$

$$\mathcal{D}_{SC} = -\frac{1}{2\tau_{sc}} \sum_{k=1}^3 [S_{ck}, [S_{ck}, \rho]]. \quad (8)$$

Assuming that the nuclear spin relaxation is dominated by dipole-dipole interaction between neighbouring nuclei, Wangness-Bloch-Redfield theory states that the dissipa-

tors take the form^{25,31–33}

$$\mathcal{D}_1 = -\frac{1}{3\tau_{n1}} \sum_{k=1}^3 [I_{1k}, [I_{1k}, \rho]], \quad (9)$$

$$\mathcal{D}_2 = -\frac{1}{3\tau_{n2}} \sum_{k=1}^3 [I_{2k}, [I_{2k}, \rho]]. \quad (10)$$

B. Lie algebraic approach

The recombination of VB holes and CB electrons require a special mathematical treatment. The process of holes recombining into doubly occupied traps and leaving a singly occupied one is represented by the \mathcal{D}_P dissipator. The SDR dissipator \mathcal{D}_{SDR} , the central subject of our discussion, accounts for the spin dependent capture of a CB electron into a singly occupied trap creating a doubly occupied one. The dissipators \mathcal{D}_P and \mathcal{D}_{SDR} can be conveniently expanded as the superposition of the elements of an internal space of Hermitian matrices that span the space of the four subspaces. This way of proceeding has many advantages. First, it easily helps avoid including spurious coherences, reducing the number of unknowns. Second, the internal product allows expressing any operator in a simple way and enables working out the dynamical equations of the system. And third, it considerably simplifies building both dissipators. The internal space is constituted of the following elements

$$\Lambda = \{p, S_k, U_{k,j,i}, V_{j,i}\} \\ = \{\lambda_1, \lambda_2, \dots, \lambda_d\}, \quad i, j, k = 0, 1, 2, 3, \quad (11)$$

where $d = 85$ is the dimension of the algebra. The previous operators are explicitly given by

$$p = 1_{1 \times 1} \oplus 0_{2 \times 2} \oplus 0_{8 \times 8} \oplus 0_{4 \times 4}, \quad (12)$$

$$S_k = 0_{1 \times 1} \oplus (s_k) \oplus 0_{8 \times 8} \oplus 0_{4 \times 4}, \quad (13)$$

$$U_{k,j,i} = 0_{1 \times 1} \oplus 0_{2 \times 2} \oplus (s_k \otimes s_j \otimes s_i) \oplus 0_{4 \times 4}, \quad (14)$$

$$V_{j,i} = 0_{1 \times 1} \oplus 0_{2 \times 2} \oplus 0_{8 \times 8} \oplus (s_j \otimes s_i), \quad (15)$$

where $i, j, k = 0, 1, 2, 3$. In this notation k is related to the electron spin and i and j to the nuclear spin. The s_k spin matrices follow the standard commutation rules

$$[s_i, s_j] = i\hbar \sum_k \epsilon_{i,j,k} s_k, \quad i, j, k = 1, 2, 3, \quad (16)$$

and $s_0 = (1/2)1_{2 \times 2}$ is half the identity matrix. The population of VB holes is represented by the operator p . The population of CB electrons is $n = 2S_0$ and S_k with $k = 1, 2, 3$ are the spin components of CB electrons. The spin matrices for Ga^{2+} centers are given by

$$S_{ck} = 4U_{k,0,0}, \quad k = 1, 2, 3. \quad (17)$$

The population operators of singly and doubly occupied centers are

$$N^1 = 8U_{0,0,0}, \quad (18)$$

$$N^2 = 4V_{0,0}. \quad (19)$$

The elements of Λ form a Lie algebra and are the orthogonal elements of an inner product vector space whose inner product is given by the trace

$$(\lambda_q, \lambda_{q'}) = \text{tr} [\lambda_q^\dagger \lambda_{q'}] = \text{Tr} [\lambda_q^2] \delta_{q,q'}. \quad (20)$$

Even though one can in principle define many other different inner products for the elements of Λ , this one has the additional advantage of being closely linked to the quantum statistical average

$$\bar{O} = \text{Tr} [O\rho], \quad (21)$$

where O is any given operator in the same space as ρ and the upper bar indicates the quantum statistical average. This equation implies that the density matrix can be expanded in terms of the quantum statistical averages of the elements of Λ as

$$\rho = \sum_q \frac{1}{\text{Tr} [\lambda_q^2]} \lambda_q \bar{\lambda}_q. \quad (22)$$

Any operator can be likewise expanded in terms of the elements of Λ as

$$O = \sum_q \frac{\text{Tr} [O\lambda_q]}{\text{Tr} [\lambda_q^2]} \lambda_q. \quad (23)$$

For example, the nuclear spin operators can be written as

$$\begin{aligned} I_{1,k} &= \sum_{j,i=0}^3 \frac{\text{Tr} [I_{1,k} U_{0,j,i}]}{\text{Tr} [U_{0,j,i} U_{0,j,i}]} U_{0,j,i} \\ &= 8 \sum_{j,i=0}^3 \text{Tr} [I_{1,k} U_{0,j,i}] U_{0,j,i}, \end{aligned} \quad (24)$$

$$\begin{aligned} I_{2,k} &= \sum_{j,i=0}^3 \frac{\text{Tr} [I_{2,k} V_{j,i}]}{\text{Tr} [V_{j,i} V_{j,i}]} V_{j,i} \\ &= 4 \sum_{j,i=0}^3 \text{Tr} [I_{2,k} V_{j,i}] V_{j,i}. \end{aligned} \quad (25)$$

C. Recombination of valence band holes in paramagnetic centers

Here we build the dissipator \mathcal{D}_P for the process in which holes recombine into Ga^{2+} centers. This calculation will serve to illustrate the more complex calculation of \mathcal{D}_{SDR} . The strategy consists in projecting the well known two-charge-state kinetic equations¹⁵ onto the base Λ in order to translate them into the dissipator \mathcal{D}_P . We start from the rate equations of the two-charge-state model¹⁵

$$\frac{d}{dt} \bar{p} = -c_p \bar{p} \sum_{\beta=-3/2}^{3/2} \bar{N}_\beta^2, \quad (26)$$

$$\frac{d}{dt} \bar{N}_{\alpha,\beta}^1 = \frac{1}{2} c_p \bar{p} \bar{N}_\beta^2, \quad (27)$$

$$\frac{d}{dt} \bar{N}_\beta^2 = -c_p \bar{p} \bar{N}_\beta^2, \quad (28)$$

where $\bar{p} = \text{Tr}[p\rho]$ is the quantum statistical average population of VB holes. The capture coefficient for holes is $c_p = 1/N_0 \tau_h$ where N_0 is the total number of centers in the sample and τ_h is the hole recombination time in the high excitation power regime. The populations of singly and doubly occupied centers $\bar{N}_{\alpha,\beta}^1$ and \bar{N}_β^2 are associated with the population operators $N_{\alpha,\beta}^1$ and N_β^2 . The subscripts $\alpha = -1/2, 1/2$ and $\beta = -3/2, -1/2, 1/2, 3/2$ tag the bound electron and nuclear spin states $|\alpha, \beta\rangle$ and $|\beta\rangle$ in singly and double charged centers, respectively. Note that whereas doubly charge states are indexed by the electron spin subscript α , singly charged centers are not, because in the latter, both electrons form a singlet state, rendering the electron spin index irrelevant. The singly occupied population operator is thus given by

$$N_{\alpha,\beta}^1 = \text{diag} \left(\overbrace{0}^p, \overbrace{0,0}^{S_k}, \overbrace{0, \dots, 0, 1, 0, \dots}^{U_{k,j,i}}, \overbrace{0, 0, 0, 0}^{V_{j,i}} \right), \quad (29)$$

where the 1 is in the entry corresponding to the state $|\alpha, \beta\rangle$. Similarly, the doubly occupied population operator is

$$N_\beta^2 = \text{diag} \left(\overbrace{0}^p, \overbrace{0,0}^{S_k}, \overbrace{0,0,0,0,0,0,0,0}^{U_{k,j,i}}, \overbrace{0, \dots, 1, \dots, 0}^{V_{j,i}} \right), \quad (30)$$

where the 1 is located in the entry associated to the state $|\beta\rangle$.

Whilst the rate equations (26)-(28) merely deal with the density matrix populations, the elements of Λ are of a more general nature and also involve off-diagonal entries of the density matrix. Hence, merely projecting the rate equations onto Λ does not suffice to get the most general form of the dissipator; it is further necessary to demand that the projected equations comply with basic requirements as isotropy of space, spin conservation and the usual tensor transformation rules. Following the

procedure above, we obtain the set of kinetic equations

$$\frac{d}{dt}\bar{p} = -4c_p\bar{p}\bar{V}_{0,0}, \quad (31)$$

$$\frac{d}{dt}\bar{U}_{k,j,i} = \frac{1}{2}\delta_{k,0}c_p\bar{p}\bar{U}_{0,j,i}, \quad (32)$$

$$\frac{d}{dt}\bar{V}_{j,i} = -c_p\bar{p}\bar{V}_{j,i}. \quad (33)$$

By projecting the right hand side of (31)-(33) onto the elements of Λ via Eq. (23), we get the explicit form of the dissipator

$$\begin{aligned} \mathcal{D}_P = & -(4c_p\bar{p}\bar{V}_{0,0})p + \frac{1}{8}\left(\frac{1}{2}\sum_{j,i=0}^3\bar{p}\bar{U}_{0,j,i}\right)U_{0,j,i} \\ & - \frac{1}{4}\left(\sum_{j,i=0}^3\bar{p}\bar{V}_{j,i}\right)V_{j,i}. \end{aligned} \quad (34)$$

This dissipator generates the rate equations (31)-(33) when plugged into the master equation (1).

D. Spin dependent recombination of conduction band electrons

Now we turn to the discussion of the spin dependent recombination dissipator \mathcal{D}_{SDR} . We analyze two different sets of rate equations. The first one was presented in Refs. [20] and [25]. Even though these rate equations allow to reproduce many of the features of the spin dynamics in GaAsN, they fail to replicate the width and the effective magnetic field as functions of the illumination power. Here we show that, due to their structure, they artificially alter correlations between the bound electrons and nuclei in Ga^{2+} centers during the recombination process. These rate equation are

$$\frac{d}{dt}\bar{n}_\alpha = -c_n\bar{n}_\alpha \sum_{\beta=-3/2}^{3/2}\bar{N}_{-\alpha,\beta}^1, \quad (35)$$

$$\frac{d}{dt}\bar{N}_{\alpha,\beta}^1 = -c_n\bar{n}_{-\alpha}\bar{N}_{\alpha,\beta}^1, \quad (36)$$

$$\frac{d}{dt}\bar{N}_\beta^2 = -c_n \sum_{\alpha=-1/2}^{1/2}\bar{n}_{-\alpha}\bar{N}_{\alpha,\beta}^1, \quad (37)$$

where $\bar{n}_\alpha = \text{Tr}[n_\alpha\rho]$ is the quantum statistical population average of CB electrons with spin equal to α . The corresponding population operators are given by

$$n_{-1/2} = \text{diag}\left(\overbrace{0}^p, \overbrace{1,0}^{S_k}, \overbrace{0,0,0,0,0,0,0,0}^{U_{k,j,i}}, \overbrace{0,0,0,0}^{V_{j,i}}\right), \quad (38)$$

$$n_{1/2} = \text{diag}\left(\overbrace{0}^p, \overbrace{0,1}^{S_k}, \overbrace{0,0,0,0,0,0,0,0}^{U_{k,j,i}}, \overbrace{0,0,0,0}^{V_{j,i}}\right), \quad (39)$$

In the rate $-c_n\bar{n}_{-\alpha}\bar{N}_{\alpha,\beta}^1$, the opposite signs of the spin subscript promote the recombination of CB electrons onto traps whose bound electrons have oppositely oriented spin. The capture coefficient for CB electrons is $c_n = 1/N_0\tau^*$ where τ^* is the electron recombination time in the low excitation power regime.

Following the same procedure as in the previous section, we project these equation on the base Λ . The resulting rate equations read

$$\frac{d}{dt}\bar{S}_k = -4c_n \sum_{k',k''=0}^3 \bar{S}_{k'}Q_{k,k',k''}^\top \bar{U}_{k'',j,i}, \quad (40)$$

$$\frac{d}{dt}\bar{U}_{k,j,i} = -c_n \sum_{k',k''=0}^3 \bar{S}_{k'}Q_{k,k',k''}^\top \bar{U}_{k'',j,i}, \quad (41)$$

$$\frac{d}{dt}\bar{V}_{j,i} = 2c_n \sum_{k',k''=0}^3 \bar{S}_{k'}Q_{0,k',k''}^\top \bar{U}_{k'',j,i}, \quad (42)$$

and yield the dissipator

$$\begin{aligned} \mathcal{D}_{SDR} = & -2 \sum_{k=0}^3 \left(4c_n \sum_{k',k''=0}^3 \bar{S}_{k'}Q_{k,k',k''}^\top \bar{U}_{k'',j,i} \right) S_k \\ & - 8 \sum_{k,j,i=0}^3 \left(c_n \sum_{k',k''=0}^3 \bar{S}_{k'}Q_{k,k',k''}^\top \bar{U}_{k'',j,i} \right) U_{k,j,i} \\ & + 4 \sum_{j,i=0}^3 \left(2c_n \sum_{k',k''=0}^3 \bar{S}_{k'}Q_{0,k',k''}^\top \bar{U}_{k'',j,i} \right) V_{j,i}, \end{aligned} \quad (43)$$

where the matrices $Q_{k,k',k''} = (\mathbb{Q}_k)_{k',k''}$ are given by

$$\mathbb{Q}_0 = \begin{pmatrix} 1 & 0 & 0 & 0 \\ 0 & -1 & 0 & 0 \\ 0 & 0 & -1 & 0 \\ 0 & 0 & 0 & -1 \end{pmatrix}, \quad \mathbb{Q}_1 = \begin{pmatrix} 0 & 1 & 0 & 0 \\ -1 & 0 & 0 & 0 \\ 0 & 0 & 0 & 0 \\ 0 & 0 & 0 & 0 \end{pmatrix}, \quad (44)$$

$$\mathbb{Q}_2 = \begin{pmatrix} 0 & 0 & 1 & 0 \\ 0 & 0 & 0 & 0 \\ -1 & 0 & 0 & 0 \\ 0 & 0 & 0 & 0 \end{pmatrix}, \quad \mathbb{Q}_3 = \begin{pmatrix} 0 & 0 & 0 & 1 \\ 0 & 0 & 0 & 0 \\ 0 & 0 & 0 & 0 \\ -1 & 0 & 0 & 0 \end{pmatrix}. \quad (45)$$

They have the property of transforming as a scalar for $k=0$ and as a vector for $k \neq 0$. That is,

$$\mathbb{R}\mathbb{Q}_0\mathbb{R}^\top = \mathbb{Q}_0, \quad (46)$$

$$\mathbb{R}\mathbb{Q}_k\mathbb{R}^\top = \sum_{k'=1}^3 R_{k,k'}\mathbb{Q}_{k'}, \quad (47)$$

where $R_{k,k'} = (\mathbb{R})_{k,k'}$ is a rotation matrix. Just as the opposite signs of the electron spins in Eqs. (35)-(37), the \mathbb{Q}_k matrices are responsible for the spin selective capture of electrons. Note that while the electron spin indices k, k' and k'' are contracted through the matrix \mathbb{Q} , the ones related with the nuclear spin indices (j and i) are not. This

is an indication that, whereas the CB and bound electron spins must have opposite orientations to recombine, nuclear spin must be preserved during a capture process. A further important property of the chosen rate equations (35)-(37) and consequently of (40)-(42) is that they insure the positive definiteness of the density matrix provided that it has appropriate initial conditions. This is because the recombination rate is proportional to both n_α and $N_{-\alpha,\beta}^1$ hence preventing any of these populations to reach values below zero.

Let us investigate the impact of this dissipator in the conservation of populations, electronic spins and nuclear spins. To do so, we strip off any terms but \mathcal{D}_{SDR} of the master equation (1). Charge conservation can be directly proved by counting the overall number of negatively charged electrons, either in the CB or in the doubly charged centers, and positively charged VB holes

$$\begin{aligned} \frac{d}{dt} (\bar{p} - \bar{n} - \bar{N}^2) &= \frac{d}{dt} (\bar{p} - 2\bar{S}_0 - 4\bar{V}_{0,0}) \\ &= \text{Tr} [(p - 2S_0 - 4V_{00}) \mathcal{D}_{SDR}] = 0, \end{aligned} \quad (48)$$

where in the last term of the right hand side we have substituted the explicit form of \mathcal{D}_{SDR} . In a similar manner we can demonstrate that \mathcal{D}_{SDR} maintains a constant number of centers

$$\begin{aligned} \frac{d}{dt} (\bar{N}^1 + \bar{N}^2) &= \frac{d}{dt} (8\bar{U}_{0,0,0} + 4\bar{V}_{0,0}) \\ &= \text{Tr} [(8U_{0,0,0} + 4V_{0,0}) \mathcal{D}_{SDR}] = 0. \end{aligned} \quad (49)$$

Electronic spin conservation also holds

$$\begin{aligned} \frac{d}{dt} (\bar{S}_k + \bar{S}_{ck}) &= \frac{d}{dt} (\bar{S}_k + 4\bar{U}_{k,0,0}) \\ &= \text{Tr} [(S_k + 4U_{k,0,0}) \mathcal{D}_{SDR}] = 0. \end{aligned} \quad (50)$$

Nuclear spin is preserved as well because, substituting

$$\begin{aligned} \frac{d}{dt} (2\bar{U}_{0,j,i} + \bar{V}_{j,i}) &= \text{Tr} [(2U_{0,j,i} + V_{j,i}) \mathcal{D}_{SDR}] = 0, \\ & \quad (51) \end{aligned}$$

in $d/dt((\bar{I}_{1,k} + \bar{I}_{2,k}) = \text{Tr}[(I_{1,k} + I_{2,k})\mathcal{D}_{SDR}]$, using Eqs. (24)-(25) and $2 \text{Tr}[I_{1,k}U_{0,j,i}] = \text{Tr}[I_{2,k}V_{j,i}]$ we obtain

$$\frac{d}{dt} (\bar{I}_{1,k} + \bar{I}_{2,k}) = 0. \quad (52)$$

Eq. (51), however, is of a more general character than the simple nuclear spin conservation. While (52) implies the conservation of only three quantities, (51) implies the conservation of sixteen. These quantities, which have the form $2\bar{U}_{0,j,i} + \bar{V}_{j,i}$, correspond to those elements of the density matrix that encode the spin nuclear structure. It could be said then that Eq. (51) means that the entire nuclear structure, is preserved during the spin selective recombination of an electron. Figure 2 shows center, electronic spin and nuclear spin conservation. All

four panels show a situation where initial spin polarized CB electrons ($n_{-1/2} = 0.22N_0$, $n_{-1/2} = 0.18N_0$) recombine into an ensemble of singly occupied centers with inhomogeneously populated nuclear states ($N_{-1/2,-1/2} = N_{-1/2,1/2} = N_{1/2,3/2} = 0.2$, $N_{-1/2,-3/2} = 0.08$, $N_{-1/2,3/2} = 0.1$, $N_{1/2,-3/2} = 0.02$, $N_{1/2,1/2} = 0.1$). The solid blue line and the solid orange line correspond to singly and doubly occupied centers. The thick green line represents the sum of singly and doubly occupied centers. We observe that the number of centers, the electronic spin and the nuclear spin are conserved in Figs. (2) (a), (b) and (c) respectively.

At first glance, it would seem that the conditions of charge conservation (48), center conservation (49), electronic spin conservation (50) and nuclear spin structure conservation (51) would suffice to completely define the spin selective capture of a CB electron. A closer inspection reveals that this is far from true. There are 19 elements of the singly charged center density matrix $\bar{U}_{k,j,i}$ encompassed by the conservation conditions: population $N^1 = 8\bar{U}_{0,0,0}$, electronic spin $\bar{S}_{ck} = 4\bar{U}_{k,0,0}$ ($k = 1, 2, 3$) and nuclear spin structure $\bar{U}_{0,j,i}$ ($i, j = 0, 1, 2, 3$ $i \neq 0 \vee j \neq 0$). Thus, we have overlooked the 45 density matrix coefficients $\bar{U}_{k,j,i}$ where $k \neq 0 \wedge (j \neq 0 \vee i \neq 0)$. These are in fact associated with the electron-nucleus spin correlation. Conditions (49), (50) and (51) in all cases entail the balance between two reservoirs. In Eqs. (49) and (51) the exchange occurs between singly and doubly occupied centers to maintain populations and nuclear spins constant. The overall electron spin is kept unaltered through the exchange between CB electrons and center bounded electrons in Eq. (50). In contrast, electron-nucleus spin correlation in Eq. (36) merely build up in singly occupied centers due to spin selective recombination. The correlation unbalance stems from Eqs. (35)-(37) where the recombination rate is modulated by the population in each nuclear state. Electrons are more likely to recombine to highly populated nuclear states consequently distorting the electron-nucleus spin correlation. It becomes obvious that the rate equations (40)-(42), but most particularly (36), are beset with a problem when one comes to realize the HFI is precisely one of the many possible electron-nucleus spin correlations. As electrons recombine the HFI is altered, among other correlations, and the ratio between the Zeeman interaction and the HFI is artificially overturned. It is hardly surprising that the width, that strongly depends on this ratio, is incorrectly reproduced by the model. This fact can be verified in Fig. (2) where the HFI is plotted as a function of time. Evidently the HFI is zero for doubly occupied traps (solid orange line) since electrons are forming a singlet state that has vanishing correlation with the nuclear spin. In contrast, the HFI for singly occupied centers varies with time (blue solid line), therefore, the total correlation can not be constant (thick green line superimposed to the solid blue line).

The simplest approach to solve this problem is simply setting to zero the group of equations that alter the

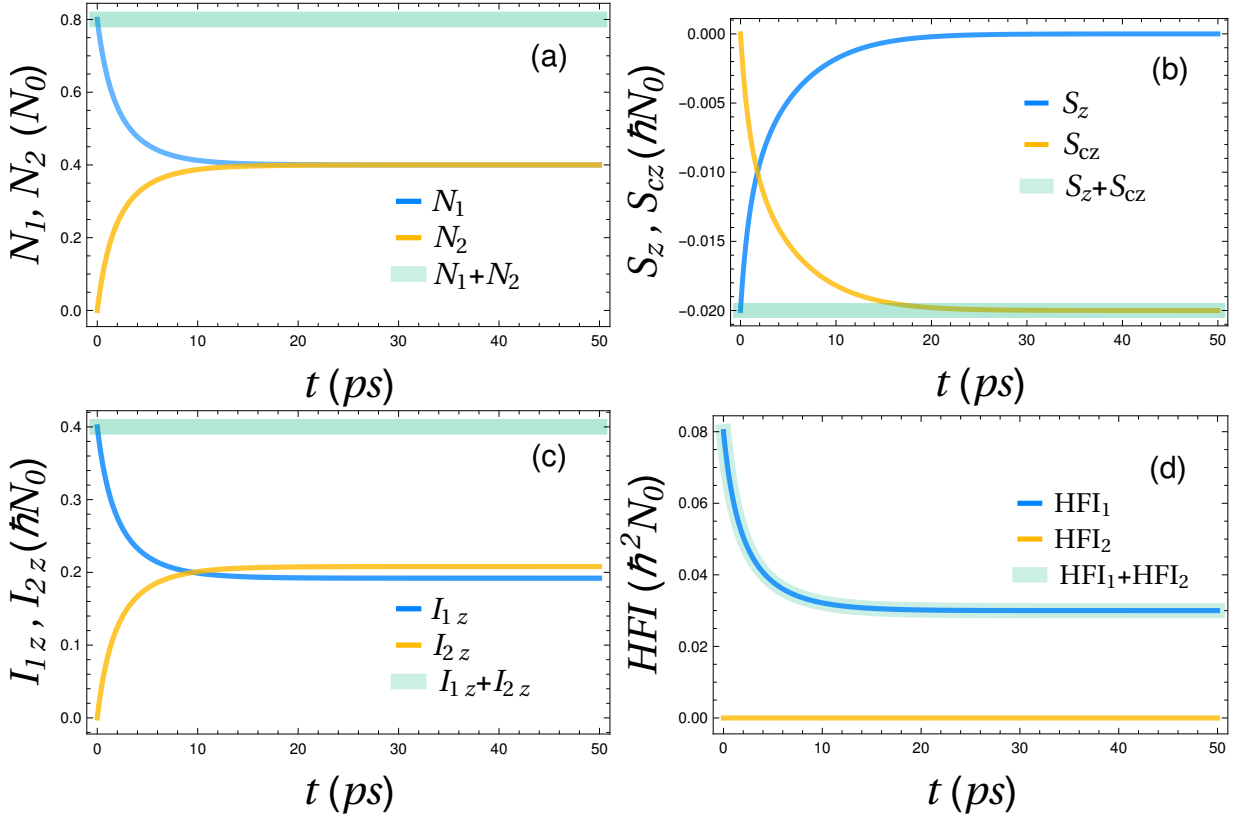


Figure 2. (a) Number of singly and doubly occupied centers N_1 and N_2 as a function of time. (b) Electronic spin of singly and doubly occupied centers S_z and S_{cz} as a function of time. (c) Nuclear spin of singly and doubly occupied centers I_{1z} and I_{2z} as a function of time. (d) Hyperfine interaction as a function of time for singly and doubly occupied centers respectively. The blue and orange solid lines correspond to singly and doubly occupied centers. The thick green line is the sum of singly and doubly occupied centers. The calculation was performed only taking into account the SDR dissipator of Eq. (43) for the following initial populations $n_{-1/2} = 0.22N_0$, $n_{1/2} = 0.18N_0$, $N_{-1/2,-1/2} = N_{-1/2,1/2} = N_{1/2,3/2} = 0.2$, $N_{-1/2,-3/2} = 0.08$, $N_{-1/2,3/2} = 0.1$, $N_{1/2,-3/2} = 0.02$, $N_{1/2,1/2} = 0.1$.

electron-nucleus correlations without tampering with the spin dependent recombination. In other words, we have to replace Eq. (41) by

$$\frac{d}{dt}\bar{U}_{k,j,i} = -c_n\mu_{k,j,i} \sum_{k',k''=0}^3 \bar{S}_{k'}Q_{k,k',k''}\bar{U}_{k'',j,i}, \quad (53)$$

where

$$\mu_{k,j,i} = \begin{cases} 1, & k = 0 \vee (k \neq 0 \wedge j = 0 \wedge i = 0), \\ 0, & k \neq 0 \wedge (j \neq 0 \vee i \neq 0). \end{cases} \quad (54)$$

With this modification the \mathcal{D}_{SDR} dissipator takes the

form

$$\begin{aligned} \mathcal{D}_{SDR} = & -2 \sum_{k=0}^3 \left(4c_n \sum_{k',k''=0}^3 \bar{S}_{k'}Q_{k,k',k''}^\top \bar{U}_{k'',j,i} \right) S_k \\ & - 8 \sum_{k,j,i=0}^3 \mu_{k,j,i} \left(c_n \sum_{k',k''=0}^3 \bar{S}_{k'}Q_{k,k',k''} \bar{U}_{k'',j,i} \right) U_{k,j,i} \\ & + 4 \sum_{j,i=0}^3 \left(2c_n \sum_{k',k''=0}^3 \bar{S}_{k'}Q_{0,k',k''}^\top \bar{U}_{k'',j,i} \right) V_{j,i}, \quad (55) \end{aligned}$$

Working back the population rate equations we find that the only change occurs in in Eq. (36) that now takes the form

$$\begin{aligned} \frac{d}{dt}\bar{N}_{\alpha,\beta}^1 = & -\frac{c_n}{8} \sum_{\beta'=-3/2}^{3/2} (\bar{n}_{-\alpha}\bar{N}_{\alpha,\beta'}^1 - \bar{n}_{\alpha}\bar{N}_{-\alpha,\beta'}^1) \\ & - \frac{c_n}{2} \sum_{\alpha'=-1/2}^{1/2} \bar{n}_{-\alpha'}\bar{N}_{\alpha',\beta}^1. \quad (56) \end{aligned}$$

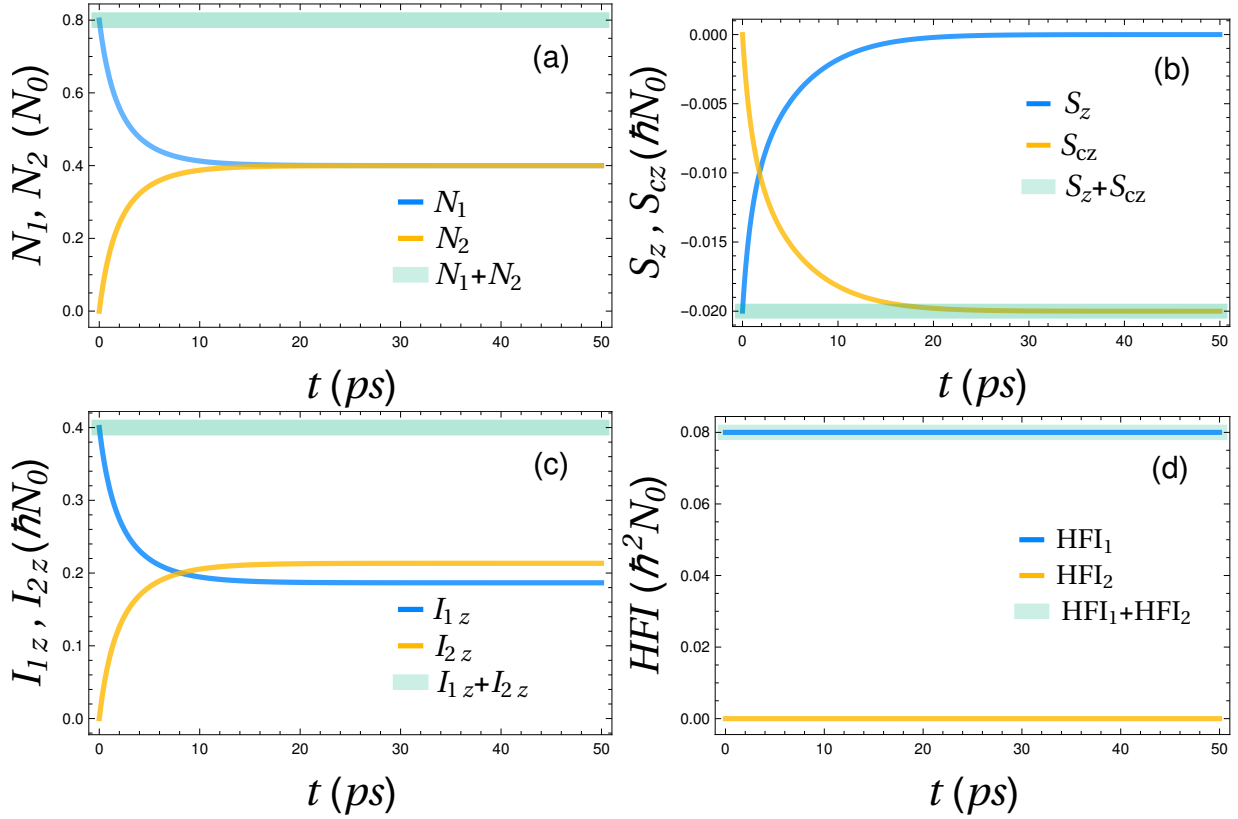


Figure 3. (a) Number of singly and doubly occupied centers N_1 and N_2 as a function of time. (b) Electronic spin of singly and doubly occupied centers S_z and S_{cz} as a function of time. (c) Nuclear spin of singly and doubly occupied centers I_{1z} and I_{2z} as a function of time. (d) Hyperfine interaction as a function of time for singly and doubly occupied centers. The blue and orange solid lines correspond to singly and doubly occupied centers respectively. The thick green line is the sum of singly and doubly occupied centers. The calculation was performed only taking into account the SDR dissipator of Eq. (55) for the following initial populations $n_{-1/2} = 0.22N_0$, $n_{1/2} = 0.18N_0$, $N_{-1/2,-1/2} = N_{-1/2,1/2} = N_{1/2,3/2} = 0.2$, $N_{-1/2,-3/2} = 0.08$, $N_{-1/2,3/2} = 0.1$, $N_{1/2,-3/2} = 0.02$, $N_{1/2,1/2} = 0.1$.

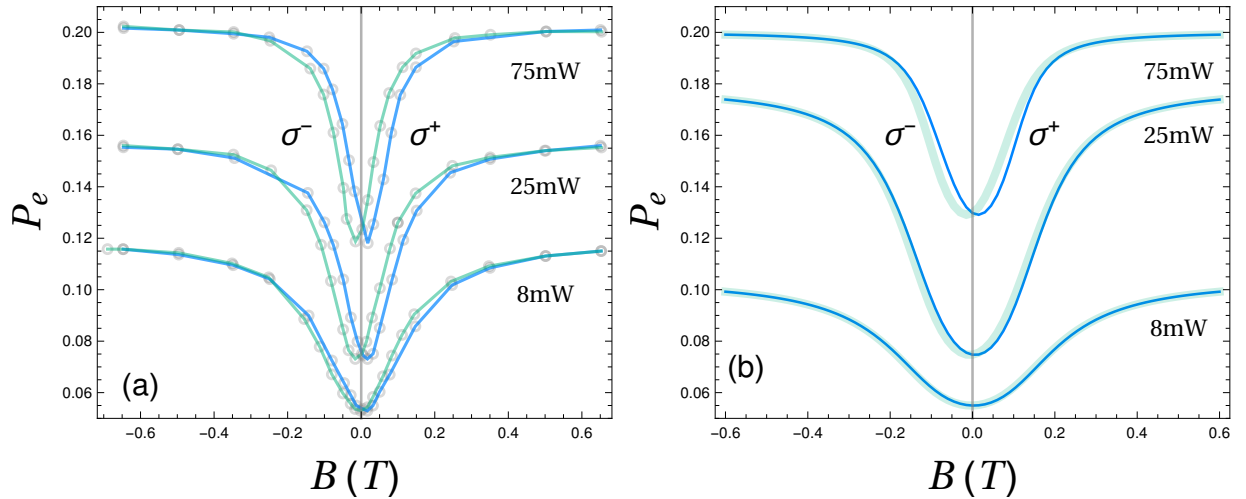


Figure 4. (a) Experimental and (b) theoretical results for the degree of circular polarization as a function of the Faraday configuration magnetic field B_z . In panel (a) the gray circles indicate the experimental points and the solid lines are a guide to the eye. Both panels show the curves corresponding to the photoluminescence degree of circular polarization under right circularly polarized excitation (σ^+ , blue solid lines) and left circularly polarized excitation (σ^- , green solid lines).

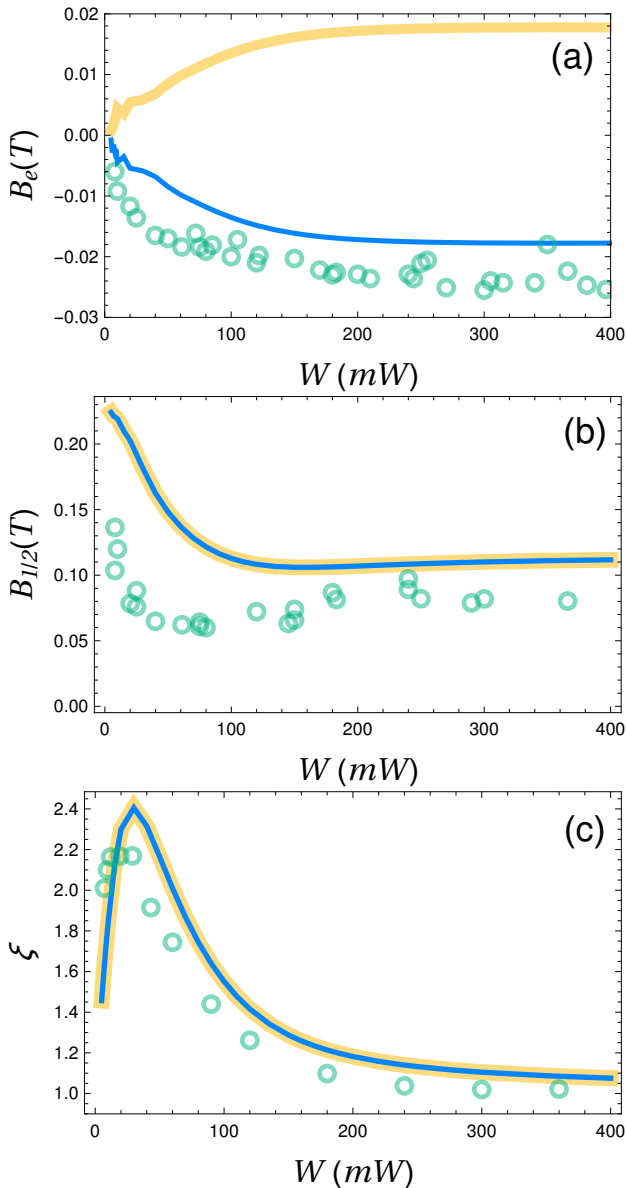


Figure 5. (a) Effective magnetic field B_e as a function of the illumination power. (b) Half width $B_{1/2}$ as a function of illumination power. (d) ξ as a function of the illumination power. The solid blue and orange lines represent the theoretical calculations for right and left circularly polarized light respectively. The green circles correspond to the experimental results.

Because the structures of (35) as well as that of (41) for $k \neq 0 \wedge j = 0 \wedge i = 0$ were not modified, the spin selective capture of electrons remains unaffected keeping the essential properties of the two-charge-state model. The first term in the right hand side of the previous equation is antisymmetric in the electronic spin index and hence, gives rise to the spin dependent capture of electrons. By itself, it does not change the overall population of singly occupied centers but instead shifts the occupation number to the bound electron spin states that have

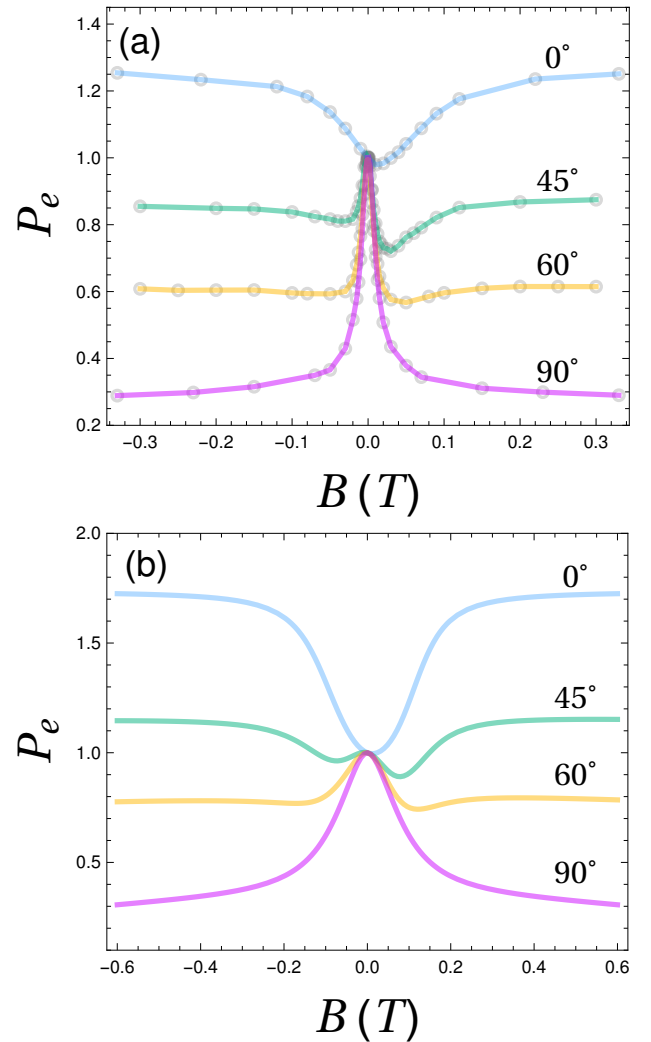


Figure 6. (a) Experimental and (b) theoretical results for degree of circular polarization as a function of an oblique magnetic field for diverse magnetic field orientations. The incidence line is perpendicular to the sample and the angles are measured with respect this orientation.

the same spin orientation as the majority of the CB electrons. The second term, on the other hand, is symmetric in the electronic spin index and therefore is responsible of the population reduction following the capture of an electron. These terms have such symmetries that all the nuclear states are depopulated at the same speed keeping the electron-nucleus spin correlation constant. It should be stressed that even though (55) gives very good results, it is not the only possible dissipator that one can think of in order to guarantee constant electron and nuclear spin correlations. In Appendix A we present the most general form that this dissipator has to take to ensure correlation conservation.

The new dissipator (55) in any of its forms is not without problems. From the structure of (56), it is clear that it can not ensure the positive definiteness of the density matrix because, contrary to (36), the recombination rate

might not become zero once the whole population of a given state is depleted. In simple terms, if the nuclear sates have different populations and depopulate at the same velocity, at least one of them is going to run out of electrons before the others. It is therefore impossible to simultaneously endow the dissipator with positive definiteness and constant electron-nucleus correlation. To circumvent this difficulty we have verified in every calculation the positive definiteness of the density matrix, i.e., that populations are in fact positive. *comment* : how this is achieved? Is it pure chance that in this case the population stay positive or there is something built-in to prevent it?

To illustrate the dynamics of these conservation principles under the action of the dissipator (55), in Fig. 3 we show the time-dependence of the number of centers, electronic spins, nuclear spins and electron-nucleus correlations as functions of time for initially non homogeneously occupied electronic and nuclear spin states. As indicated by the orange solid lines, we observe that overall values of these quantities are preserved over a spin dependent recombination process. Particular attention should be paid to Fig. 3d where it is shown that, unlike (43), the dissipator (55) preserves the average of the HFI. It should be noted that in this figure we only plot one of the 45 possible electron-nucleus correlations. The remaining 44 correlations are also preserved although they are not shown here.

III. RESULTS AND DISCUSSION

Now we want to study in more detail the effect of the new SDR dissipator \mathcal{D}_{SDR} in Eq.(55) in measurable quantities as the DCP $P_e(B_z)$ and the PL intensity $J(B_z)$. In particular, we intend to verify if the new structure of \mathcal{D}_{SDR} is capable of capturing the main experimental features of the shift B_e and width $B_{1/2}$ as functions of the illumination power. Both, the DCP and the PL intensity yield similar curves for the shift and width as functions of power, therefore, we only concentrate in the behaviour of the B_e and $B_{1/2}$ that stem from $P_e(B_z)$. To further examine the performance of the model in reproducing experimental results we contrast the measurements of the DCP in oblique magnetic fields²⁴ This test is of particular interest because under a tilted magnetic field $P_e(B_z)$ strongly depends on the width and the shift. Moreover, previous models based on simpler nuclear structures with spin $1/2$ ²⁴ fail to reproduce some of the features. In addition, the quantities that were correctly reproduced by the old SDR dissipator \mathcal{D}_{SDR} in Eq.(43) are expected to maintain their previous trends.

Using the selection rules of GaAs³⁰ it can easily be proven that the DCP is related to the degree of spin polarization of CB electrons as

$$P_e = \frac{P_i \bar{S}_z(t)}{3 \bar{n}(t)}, \quad (57)$$

where P_i is a phenomenological factor¹⁷. To extract the expectation values of CB electrons spin and population $\bar{S}_z(t)$ and $\bar{n}(t)$ we introduce the operators S_z and n into Eq. (21) along with the expansion of the density matrix $\rho(t)$ (22). This procedure casts $\bar{S}_z(t)$ and $\bar{n}(t)$, and any other observable, into the convenient form of a function of the quantum-statistical averages $\bar{\lambda}_q(t)$. This way of expressing the quantum-statistical averages is specially suitable to make calculations in an integrated manner with the master equation of the density matrix. It only remains to transform the master equation (1), a set of differential equation for the elements of $\rho(t)$, into a series of differential equations for the quantum-statistical averages $\bar{\lambda}_q$. This is easily achieved through multiplying the master equation by the operator λ_q and taking the trace²⁵

$$\begin{aligned} \dot{\bar{\lambda}}_q &= \frac{i}{\hbar} \text{Tr} [[H, \lambda_q] \rho(t)] + \text{Tr} [\mathcal{D}\lambda_q] \\ &= F_q(\lambda_1, \lambda_2, \dots, \lambda_d, t). \end{aligned} \quad (58)$$

Replacing the density matrix with the expansion (22) we are led to the result

$$\begin{aligned} F_q(\lambda_1, \lambda_2, \dots, \lambda_d, t) \\ = \frac{i}{\hbar} \sum_{q'=1}^d \frac{\bar{\lambda}_{q'}}{\text{Tr}[\lambda_{q'}^2]} \text{Tr} [H [\lambda_q, \lambda_{q'}]] + \text{Tr}[\mathcal{D}\lambda_q]. \end{aligned} \quad (59)$$

The $d = 85$ differential equations that arise from (58) are in fact the new rate equations that generalize the two-charge-state model²⁵. Any quantum-statistical average is calculated by numerically solving the system of ordinary differential equations (58), allowing it to reach steady state conditions and plugging the solution into Eq. (21).

In particular, here we contrast three specific theoretical results with its experimental counterparts: B_e , $B_{1/2}$ and ξ as functions of the illumination power where

$$\xi = P_e(\infty)/P_e(0). \quad (60)$$

In the previous equation $P_e(0)$ is the DCP at zero longitudinal magnetic field and $P_e(\infty)$ is the DCP at infinite longitudinal magnetic field. At infinite magnetic field, the Zeeman interaction overwhelms the HFI decoupling the electronic and nuclear spins in Ga²⁺ centers. In these conditions the system behaves as if there was no HFI and could in principle be described solely by the two-charged state model. Hence ξ parametrizes the degree of participation of the HFI in the SDR process.

To start, Fig. 4 shows a comparison of the experimental and theoretical results of P_e as a function of the Faraday configuration magnetic field for various illumination powers. The parameters that best fit the experimental data are the following: $N_0 = 2.24 \times 10^{15} \text{cm}^{-3}$, $\tau^* = 5\text{ps}$, $\tau_h = 30\text{ps}$, $\tau_s = 120\text{ps}$, $\tau_{sc} = 2100\text{ps}$, $\tau_{n1} = 2100\text{ps}$, $\tau_{n2} = 5\text{ps}$, $G_0 = 2.0 \times 10^{23} \text{mW}^{-1} \text{s}^{-1} \text{cm}^{-3}$, $P = 0.18$, $P_i = 0.3$, $g = 1$, $g_c = 1.7$ and $A = 0.0690 \text{cm}^{-1}$. In contrast with the results shown in Fig. 1 or in Ref. [25], the

effective magnetic field and the half width saturate at approximately 150mW. This is confirmed in Fig. 5 where B_e , $B_{1/2}$ and ξ are plotted as functions of the illumination power W . The effective magnetic field B_e and the mean width $B_{1/2}$ have been extracted from the $P_e(B_z)$ curves by means of the golden section search algorithm with a tolerance of $1\mu\text{T}$. $P_e(0)$ and $P_e(\infty)$, necessary to calculate ξ , are byproducts of the algorithm used to determine $B_{1/2}$. The experimentally determined effective magnetic field B_e in panel (a) of Fig. 5 (green circles) starts at 0T and decreases steadily with power down to -25mT at approximately 150mW. Similarly, the theoretical results for B_e (solid blue lines) yield a monotone decreasing function of power that saturates at approximately -15mT at a power of 150mW for left circularly polarized light ($P = 0.18$). Under right circularly polarized excitation ($P = -0.18$) we obtain the opposite result: the effective magnetic field increases with power until it reaches a point of saturation at $+0.15\text{mT}$ for a power of 150mW (solid orange line). Even though there is a difference of 10mT between the experimental and theoretical saturation effective magnetic fields, both trends are qualitatively comparable. It is unlikely that this difference is due to the parameter choice since a vast number of parameter combinations yield $|B_e| = \pm 15\text{mT}$ as the maximum obtainable value for the effective magnetic field. For instance, following a similar procedure as the one described in Ref. [25], the B_e isolines as a function of the nuclear spin relaxation times τ_{n1} and τ_{n2} give a maximum value of approximately 15mT for $\tau_{n1} = 2100\text{ps}$ and $\tau_{n2} < 5\text{ps}$. It is more probable that this difference is due to the particular choice of dissipator made in (55). As we mentioned above and in appendix A, the electron nucleus spin correlation conservation condition alone is not sufficient to completely define the SDR dissipator. The behaviour of the calculated mean width $B_{1/2}$ as a function of power (solid blue line), shown in Fig. 5 (b), exhibits a very good qualitative and quantitative agreement with the experimental data (green circles). At low powers we observe the largest discrepancy between experimental and theoretical results: the theoretical values of ξ underestimate by a few tens of mT the experimental ones. Both trends are quite similar: $B_{1/2}$ decreases monotonically until it saturates at approximately 200mT. The curve displayed by the theoretical values of ξ as a function of illumination power seen in Fig. 5 (c) is also in very good agreement with the experimental data. This curve had been correctly reproduced by previous models²⁵. This is to be expected since ξ solely depends on two extreme situations: the first, when the HFI is the dominant interaction ($B_z = 0$) and the second, when the Zeeman energy prevails over the HFI ($B_z \rightarrow \infty$). It does not depend however on which value of the magnetic field B_z the HFI becomes irrelevant and on how steep this transition is. Thus, the agreement between the experimental and theoretical results for ξ is an indication that the new SDR dissipator captures the correct behaviour of P_e at both ends, $B_z = 0$ and $B_z \rightarrow \infty$, but at the same

time modifies the magnetic field value at which the electrons and nuclei in Ga^{2+} centers transition from having a strong hyperfine coupling to being decoupled.

To conclude our discussion and further test the capabilities of the new SDR dissipator, we move on to the experimental results of the DCP P_e in an oblique magnetic field²⁴. Figure 6 (a) shows the experimental data of the P_e as a function of the magnitude of a tilted magnetic field for various magnetic field orientations. Once again, here we attain a very good agreement with the theoretical calculations plotted in Fig. 6 (b). At 90° (solid purple line) the P_e exhibits the typical Lorentzian curve of the Hanle effect observed in Voigt configuration¹⁰. In contrast, at 0° (solid blue line) we observe the characteristic inverted Lorentzian curve corresponding to the amplification of the spin filtering effect¹⁷. The intermediate angles (45° and 60°) yield a superposition of both functions²⁴: the upward Hanle effect Lorentzian and the downward Lorentzian corresponding to the amplification of the spin filtering effect.

IV. CONCLUSIONS

We have systematically investigated the consequences of the bogus electron-nucleus spin correlations in the spin dependent capture of electrons in Ga^{2+} paramagnetic centers. These were inadvertently incorporated in most models through the bimolecular-like terms that account for the mechanism of spin dependent recombination of CB electrons in Ga^{2+} defects. We have shown that the electron-nucleus spin correlations are responsible of the pronounced differences between the experimental and theoretical findings on the effective magnetic field B_e and width $B_{1/2}$ as functions of the illumination power. The general form of an alternative spin dependent capture mechanism that preserves electron-nucleus spin correlation has been proposed and thoroughly tested. This mechanism, embedded in the master equation for GaAsN in the form of a dissipator, yields very good agreement between theoretical and the experimental observations. particular, very good accordance is observed with experimental data concerning B_e , $B_{1/2}$ and $P_e(B_z)$.

V. ACKNOWLEDGEMENTS

We acknowledge funding from LIA CNRS-Ioffe RAS ILNACS. L.A.B. and E.L.I. thanks the Russian Foundation for Basic Research (Grants No. 17-02-00383 and No. 17-52-16020). V.K.K. acknowledges the financial support of the Government of Russia (Project No. 14.Z50.31.0021). A.K. gratefully appreciates the financial support of Departamento de Ciencias Básicas UAM-A grant numbers 2232214 and 2232215. V.G.I.S and J.C.S.S. acknowledge the total support from DGAPA-UNAM fellowship. X.M. also thanks Institut Universitaire de France. This work was supported by Programme

Investissements d'Avenir under the program ANR-11-IDEX-0002-02, reference ANR-10-LABX-0037-NEXT.

Appendix A

In order to avoid adding electron-nucleus spin correlations, the most general form of the SDR rate equations (40)-(42) should be

$$\frac{d}{dt}\bar{S}_k = \eta_k, \quad (\text{A1})$$

$$\frac{d}{dt}\bar{U}_{k,0,0} = -\frac{\eta_k}{4}, \quad k = 0, 1, 2, 3, \quad (\text{A2})$$

$$\frac{d}{dt}\bar{U}_{0,j,i} = \varphi_{j,i}, \quad j, i = 0, 1, 2, 3, / \{i = j = 0\}, \quad (\text{A3})$$

$$\frac{d}{dt}\bar{U}_{k,j,i} = 0, \quad k = 1, 2, 3, \\ i, j = 0, 1, 2, 3, / \{j = i = 0\}, \quad (\text{A4})$$

$$\frac{d}{dt}\bar{V}_{j,i} = -2\varphi_{j,i}, \quad j, i = 0, 1, 2, 3, \quad (\text{A5})$$

where η_k and $\varphi_{j,i}$ are arbitrary generation rate terms. Equation (A4) guarantees that no extra electron-nucleus spin correlation is added during the spin selective capture of an electron. The generation rates in Eqs. (A1) and (A2) are balanced to preserve electronic spin during the

recombination process. Similarly, the generation rates of Eqs. (A3) and (A5) compensate to maintain constant nuclear spin and total center population. The following supplementary constraint regarding charge conservation must be added to this system of equations

$$4\varphi_{0,0} - 2\eta_0 = 0. \quad (\text{A6})$$

If additionally we assume that the recombination process must also have the same structure as the two charged-state model then, from Eq. (40) we obtain

$$\eta_k = -4c_n \sum_{k',k''=0}^3 \bar{S}_{k'} Q_{k,k',k''}^\top \bar{U}_{k'',j,i}. \quad (\text{A7})$$

Using this equation and (A6) one may also determine $\varphi_{0,0}$. The remaining recombination rates of the form $\varphi_{j,i}$ for $j, i = 0, 1, 2, 3$ except $j = i = 0$ are undetermined and can not be derived from any conservation principle. In the rate equation (42) we made the obvious choice of setting the remaining recombination rates to

$$\varphi_{j,i} = 2c_n \sum_{k',k''=0}^3 \bar{S}_{k'} Q_{0,k',k''}^\top \bar{U}_{k'',j,i}. \quad (\text{A8})$$

This, however, is not the only possibility.

-
- ¹ D. J. Lepine, Phys. Rev. B **6**, 436 (1972).
² C. Weisbuch and G. Lampel, Solid State Communications **14**, 141 (1974).
³ D. Paget, Phys. Rev. B **30**, 931 (1984).
⁴ V. K. Kalevich, E. L. Ivchenko, M. M. Afanasiev, A. Y. Shiryayev, A. Y. Egorov, V. M. Ustinov, B. Pal, and Y. Masumoto, Journal of Experimental and Theoretical Physics Letters **82**, 455 (2005).
⁵ L. Lombez, P.-F. Braun, H. Carrère, B. Urbaszek, P. Renucci, T. Amand, X. Marie, J. C. Harmand, and V. K. Kalevich, Applied Physics Letters **87**, 252115 (2005), <https://doi.org/10.1063/1.2150252>.
⁶ V. K. Kalevich, A. Y. Shiryayev, E. L. Ivchenko, A. Y. Egorov, L. Lombez, D. Lagarde, X. Marie, and T. Amand, JETP Letters **85**, 174 (2006).
⁷ D. Lagarde, L. Lombez, X. Marie, A. Balocchi, T. Amand, V. K. Kalevich, A. Shiryayev, E. Ivchenko, and A. Egorov, physica status solidi (a) **204**, 208 (2007), <https://onlinelibrary.wiley.com/doi/pdf/10.1002/pssa.200673006>.
⁸ F. Zhao, A. Balocchi, G. Truong, T. Amand, X. Marie, X. J. Wang, I. A. Buyanova, W. M. Chen, and J. C. Harmand, Journal of Physics: Condensed Matter **21**, 174211 (2009).
⁹ X. Wang, I. A. Buyanova, F. Zhao, D. Lagarde, A. Balocchi, X. Marie, C. Tu, J. Harmand, and W. Chen, Nature materials **8**, 198 (2009).
¹⁰ V. K. Kalevich, A. Shiryayev, E. Ivchenko, M. Afanasiev, A. Egorov, V. Ustinov, and Y. Masumoto, Physica B: Condensed Matter **404**, 4929 (2009).
¹¹ H. M. Zhao, L. Lombez, B. L. Liu, B. Q. Sun, Q. K. Xue, D. M. Chen, and X. Marie, Applied Physics Letters **95**, 041911 (2009), <https://doi.org/10.1063/1.3186076>.
¹² F. Zhao, A. Balocchi, A. Kunold, J. Carrey, H. Caré, T. Amand, N. Ben Abdallah, J. C. Harmand, and X. Marie, Applied Physics Letters **95**, 241104 (2009), <https://doi.org/10.1063/1.3273393>.
¹³ X. J. Wang, Y. Puttisong, C. W. Tu, A. J. Ptak, V. K. Kalevich, A. Y. Egorov, L. Geelhaar, H. Riechert, W. M. Chen, and I. A. Buyanova, Applied Physics Letters **95**, 241904 (2009), <https://doi.org/10.1063/1.3275703>.
¹⁴ Y. Puttisong, X. J. Wang, I. A. Buyanova, H. Carre, F. Zhao, A. Balocchi, X. Marie, C. W. Tu, and W. M. Chen, Applied Physics Letters **96**, 052104 (2010), <https://doi.org/10.1063/1.3299015>.
¹⁵ E. L. Ivchenko, V. K. Kalevich, A. Y. Shiryayev, M. M. Afanasiev, and Y. Masumoto, Journal of Physics: Condensed Matter **22**, 465804 (2010).
¹⁶ A. Kunold, A. Balocchi, F. Zhao, T. Amand, N. B. Abdallah, J. C. Harmand, and X. Marie, Phys. Rev. B **83**, 165202 (2011).
¹⁷ V. K. Kalevich, M. M. Afanasiev, A. Y. Shiryayev, and A. Y. Egorov, Phys. Rev. B **85**, 035205 (2012).
¹⁸ C. T. Nguyen, A. Balocchi, D. Lagarde, T. T. Zhang, H. Carré, S. Mazzucato, P. Barate, E. Galopin, J. Gierak, E. Bourhis, J. C. Harmand, T. Amand, and X. Marie, Applied Physics Letters **103**, 052403 (2013), <https://doi.org/10.1063/1.4816970>.
¹⁹ V. K. Kalevich, M. M. Afanasiev, A. Y. Shiryayev, and A. Y. Egorov, JETP Letters **96**, 567 (2013).

- ²⁰ Y. Puttison, X. Wang, I. Buyanova, L. Geelhaar, H. Riechert, A. Ptak, C. Tu, and W. Chen, *Nature communications* **4**, 1751 (2013).
- ²¹ Y. Puttison, X. J. Wang, I. A. Buyanova, and W. M. Chen, *Phys. Rev. B* **87**, 125202 (2013).
- ²² C. Sandoval-Santana, A. Balocchi, T. Amand, J. C. Harmand, A. Kunold, and X. Marie, *Phys. Rev. B* **90**, 115205 (2014).
- ²³ E. L. Ivchenko, L. A. Bakaleinikov, and V. K. Kalevich, *Phys. Rev. B* **91**, 205202 (2015).
- ²⁴ E. L. Ivchenko, L. A. Bakaleinikov, M. M. Afanasiev, and V. K. Kalevich, *Physics of the Solid State* **58**, 1539 (2016).
- ²⁵ V. G. Ibarra-Sierra, J. C. Sandoval-Santana, S. Azaizia, H. Carrère, L. A. Bakaleinikov, V. K. Kalevich, E. L. Ivchenko, X. Marie, T. Amand, A. Balocchi, and A. Kunold, *Phys. Rev. B* **95**, 195204 (2017).
- ²⁶ S. Azaizia, H. Carrère, J. C. Sandoval-Santana, V. G. Ibarra-Sierra, V. K. Kalevich, E. L. Ivchenko, L. A. Bakaleinikov, X. Marie, T. Amand, A. Kunold, and A. Balocchi, *Phys. Rev. B* **97**, 155201 (2018).
- ²⁷ J. C. Sandoval-Santana, V. G. Ibarra-Sierra, S. Azaizia, H. Carrère, L. A. Bakaleinikov, V. K. Kalevich, E. L. Ivchenko, X. Marie, T. Amand, A. Balocchi, and A. Kunold, *The European Physical Journal Plus* **133**, 122 (2018).
- ²⁸ V. Ibarra-Sierra, J. Sandoval-Santana, S. Azaizia, H. Carrère, L. Bakaleinikov, V. Kalevich, E. Ivchenko, X. Marie, T. Amand, A. Balocchi, *et al.*, *Journal of Materials Science: Materials in Electronics* **29**, 15307 (2018).
- ²⁹ S. Chen, Y. Huang, D. Visser, S. Anand, I. A. Buyanova, and W. M. Chen, *Nature communications* **9**, 3575 (2018).
- ³⁰ F. Meier and B. P. Zakharchenya, *Optical orientation* (Elsevier, 2012).
- ³¹ R. K. Wangsness and F. Bloch, *Phys. Rev.* **89**, 728 (1953).
- ³² A. Redfield, in *Advances in Magnetic Resonance*, *Advances in Magnetic and Optical Resonance*, Vol. 1, edited by J. S. Waugh (Academic Press, 1965) pp. 1 – 32.
- ³³ G. W. Leppelmeier and E. L. Hahn, *Phys. Rev.* **142**, 179 (1966).